Weak localization and phase interference due to spin-orbit interaction in metal-doped carbon nanotubes

Junji Haruyama, Izumi Takesue, and Tetsuro Hasegawa
Aoyama Gakuin University, 6-16-1 Chitosedai, Setagaya, Tokyo 157-8572 Japan
(Received 19 March 2001; published 13 December 2001)

Electrode atoms are slightly diffused, with only about 5% volume ratio, into the top end of multiwalled carbon nanotubes (MWNT's), standing in nanopores of porous alumina membranes. Diffusion of light-mass materials (carbon and aluminum) leads to weak localization in the Altshuler-Aronov-Spivak (AAS) oscillations, which is qualitatively consistent with previous works on MWNT's. In contrast, we find that diffusion of heavy materials (gold and platinum) changes this weak localization into an antilocalization in the MWNT bulk. This effect is only observable when electrons are injected through the diffusion region and undergo a π-phase shift in their electron waves, caused by polarized injection of spin-flipped electrons due to spin-orbit interaction in the diffusion region of the MWNT bulk.

DOI: 10.1103/PhysRevB.65.033402 PACS number(s): 73.20.Fz, 71.70.Ej, 73.61.Wp

Single-walled carbon nanotubes are conducting molecular nanowires that exhibit a variety of mesoscopic phenomena. There is renewed interest in these nanostructures because their characteristics are very sensitive to materials deposited onto the tube inner space.[1] In contrast, the physical properties of multiwalled carbon nanotubes (MWNT's) have been interpreted only in terms of quantum phase interference effects of electron waves in the diffusive regime at the single-molecular level [e.g., weak localization (WL),[2–4] Altshuler-Aronov-Spivak (AAS) oscillations,[5–9] universal conductance fluctuation,[2] possible metal-insulator transition,[10] and strong spin coherence[11]]. The investigation of the correlation of such interference phenomena with dopant materials in the tube inner space or the MWNT itself has so far received no attention.

AAS oscillations and WL are the typical phase interference effects of electron waves observed in MWNT's. Constructive phase interferences in current paths encircling MWNT's with time-reversal symmetry leads to WL, when the sample size is smaller than both the phase coherence length and the localization length.[12–14] The presence of a resistance maximum and a negative magnetoresistance (MR) around zero magnetic field reflect WL in the AAS oscillations.[15] Previous works on MWNT's reported only on this type of AAS oscillations. On the other hand, the presence of a strong spin-orbit interaction (SOI) in thin metallic cylinders formed by heavy-mass atoms leads to antilocalization (AL), reflected by a resistance minimum and a positive MR around zero magnetic field, in the AAS oscillations.[16] This is because the SOI causes electron-spin flipping, thereby leading to a change of the electron phase by π.[17–19] No group, however, has yet successfully observed this electron-spin flipping and AL in the AAS oscillations in MWNT's.

In this paper, we find that the diffusion of heavy-mass atoms, deposited onto the top end of MWNT electrodes with only about 5% in volume ratio, drastically changes this WL to AL in the bulk of the MWNT's. Based on a revised Altshuler's theory, we show that the SOI, depending on the diffused atom mass and the diffusion volume ratio, is the key for understanding the WL into the AL change. We find that this phenomenon is observable only when electrons are injected through the diffusion region and is understood as a spin flipping of electron waves (i.e., phase shift by π), caused by the SOI in the diffusion region of the bulk of MWNT's.

In electrical measurements of MWNT's performed in previous works, an individual MWNT was deposited on a substrate[5,6] and gold- (Au-) finger-like electrodes were fabricated by lithography over the MWNT. Only the upper half-part of the MWNT that did not face the substrate had an interface with the electrodes. Hence, it was difficult to diffuse by annealing the electrode atoms into one entire end of the MWNT along the circumference of the NT (including the lower half-part facing the substrate). In contrast, we reported earlier on a different method to obtain the characteristics of MWNT arrays standing in nanosized diameter pores of porous alumina membranes.[7–9] In this method, after the deposition of MWNT's into the nanopores, the top ends of the standing MWNT's were exposed from the surface of alumina membranes [Fig. 1(a)] and, then, a thick electrode was directly deposited on all of the top ends [Fig. 1(b)]. Hence, diffusion of electrode atoms takes places into the entire end of the standing MWNT's. For this reason, the diffusion region of the electrode atoms forms the other nanotubelike structure on the top end of MWNT's [Fig. 1(b)]. In fact, our sample clearly exhibits the diffusion of Au atoms, deposited as an electrode material, into the top end of MWNT, as shown in Fig. 1(c).

Figure 2 shows typical MR oscillations characteristics observed in the samples with four different electrode materials. In this work, we measured a large number of MWNT's in one array sample at the same time. However, although this smears MR oscillations in some cases, we assumed that the observed characteristics were the simple superposition of the characteristic of each MWNT for the following three reasons: (1) the uniformity of the tube diameter was extremely high (e.g., half-width of distribution was less than 13%), (2) the spacing between the MWNT's was relatively large, and (3) according to Ref. 20, the characteristics of the individual MWNT's and the MWNT arrays fabricated by this method were basically consistent.

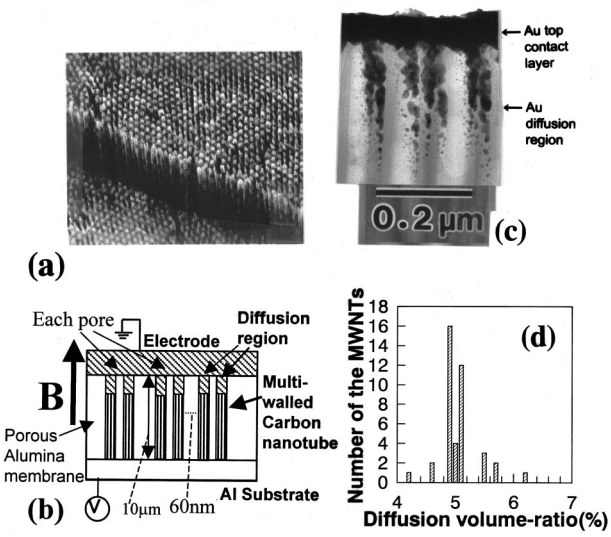

FIG. 1. (a) SEM overview image of the exposed top part of a multiwalled carbon nanotube (MWNT) array, exhibiting a high regularity. (b) Schematic cross section of the MWNT array sample. (c) Cross sectional TEM (CSTEM) image around the top end of the MWNT array with the top electrode (gold: Au). White parts mean the tube inner spaces. (d) Distribution of the diffusion volume-ratio of Au electrode, obtained from CSTEM images of one array. The total number of the MWNT's investigated is 41.

Since Fig. 2(a) exhibits the MR maximum at $B=0$ T and negative MR, the localization type is WL. This is qualitatively consistent with the previous works on AAS oscillations in MWNT's. Figure 2(b) also exhibits a MR oscillation with WL, although the decrease of MR saturates around $B=0.5$ T. On the contrary, the MR oscillations shown in Figs. 2(c) and 2(d) clearly reveal the MR minimums at $B=0$ T

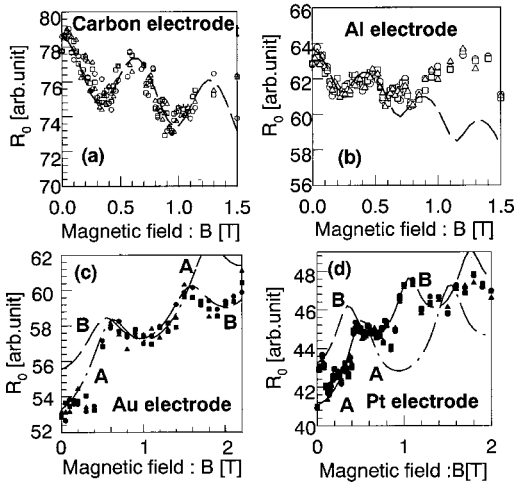

FIG. 2. Dependence of magnetoresistance (MR) oscillations on the top electrode materials. Four samples with different electrode materials [i.e., (a) carbon, (b) aluminum, (c) gold, and (d) platinum] were measured. The magnetic field was applied in parallel with the tube axis. We basically plot the three times measurement results at each magnetic field. Dashed and dotted lines are the calculation results by Eqs. (1)–(4).

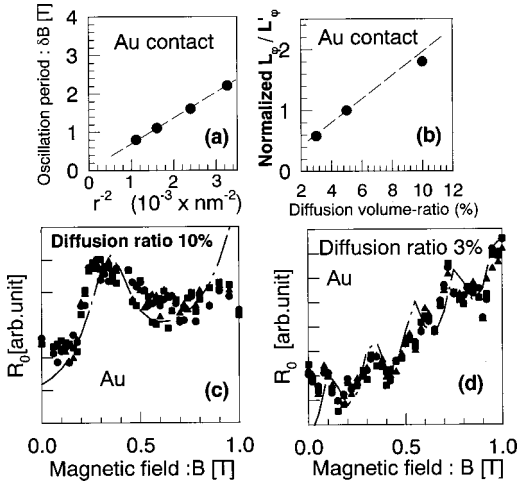

FIG. 3. (a) MR oscillation period vs square of mean tube radii. Mean tube radii of the array samples are confirmed by TEM and SEM images. (b) Normalized L_φ/L'_φ vs diffusion volume-ratio of Au atom to the MWNT. Each L_φ/L'_φ was obtained from the best data fitting to (c) and (d) by Eqs. (1)–(4), and then normalized by that for line A of the Fig. 2(c) sample with 5% ratio. (c) MR oscillation in the sample with the diffusion volume ratio 2 times higher than the Fig. 2(c) sample. Dotted line means the calculation result from Eqs. (1)–(4). (d) That with the diffusion-volume ratio 0.6 times smaller than the Fig. 2(c) sample. The smaller oscillation period is due to the larger tube radius caused by the fabrication process to get the longer tube length.

and positive MR's which imply the presence of AL, although the oscillations themselves are not clear in comparison with (a) and (b). The positive MR is in contradiction with previous works.[5,7–9]

In order to confirm the correlation between the observed MR oscillations and the AAS effect, we investigated the dependence of the oscillation period ΔB, on the MWNT radius r. Figure 3(a) shows the result, which is a linear ΔB vs r^{-2} relation with the slope value of 2.5×10^{-16} (J S/C). This is quantitatively in good agreement with the relation $\Delta B=(h/2e)/(\pi r^2)$ given by the AAS oscillation theory, with $(h/2e)/\pi\sim6.5\times10^{-16}$.

Next, we discuss the influence of the electrode materials on the type of localization observed in the AAS oscillations as suggested by the results on Fig. 2. The atomic numbers of Pt and Au are 78 and 79, respectively, whereas those of C and Al are 6 and 13. This indicates that the emergence of WL or AL strongly depends on the mass of the electrode-material atoms. Since AL is observable only in the samples with heavy-mass electrode materials (Pt and Au), this is qualitatively consistent with the previous works on thin Mg and Li cylinders,[15,16] which emphasizes the contribution of the SOI. However, it should be noticed that the diffusion region of our electrode materials is only about 5% of the volume ratio in our MWNT's. Hence, one deals with a qualitatively different phenomenon from any previous observations in thin metallic film systems, although nothing of this kind has been reported in MWNT systems.

In order to resolve this issue, we carry out a data fitting procedure based on Altshuler's equations for AAS

oscillations.[15] In Ref. 15, the equations for AAS oscillations including the contribution of the SOI can be rewritten as follows:

$$dG = -(e^2/\pi h)(2\pi r/L_s)[(1/2+\beta)Z_\Phi(L_\varphi(H)) - 3/2Z_\Phi(L'_\varphi(H))] + \alpha(H), \quad (1)$$

$$Z_\Phi(L_\varphi(H)) = \ln(L_\varphi/l) + 2\sum k_0(n(2\pi r/L_\varphi)) \times \cos[2\pi n(\Phi/(hc/2e))], \quad (2)$$

$$1/L_\varphi^2 = 1/Dt_\varphi, \quad (3)$$

$$1/L_\varphi'^2 = 1/L_\varphi^2 + 2/Dt_{so} \quad (4)$$

where L_s, β, L_φ, and L'_φ in Eq. (1) are the tube length, the constant depending on the electron-electron interaction, and the phase coherent length without and with the SOI, respectively. l, k_0, and Φ in Eq. (2) are the mean free path, the Macdonald function, and the magnetic flux ($\pi r^2 H$), respectively. D, t_φ, and t_{so} in Eqs. (3) and (4) are the diffusion constant, the relaxation time for inelastic scattering, and the relaxation time for the SOI, respectively. Here, $\alpha(H)$ in Eq. (1) represents the increase or decrease of the mean value of the conductance, depending on magnetic field H. We also neglected the contribution of magnetic field on L_φ in Eq. (3).

Equation (1) has very simple physical meaning: The first term related to $Z_\Phi(L_\varphi(H))$ basically represents the AAS oscillations without the SOI (i.e., WL), whereas the second term with $Z_\Phi(L'_\varphi(H))$ reveals the influence of SOI (i.e., AL) on the AAS oscillations, using Eq. (4). Equation (4) includes the term $1/Dt_{so}$ as the contribution of the SOI. If the SOI is very weak, t_{so} diverges to an infinite value and, hence, L_φ/L'_φ becomes "1" because of $(L_\varphi/L'_\varphi)^2 = 1 + 2(L_\varphi^2)/Dt_{so}$, leading to WL. On the contrary, if t_{so} has a finite value, L_φ/L'_φ becomes larger than "1" because of $2(L_\varphi^2)/Dt_{so} > 0$, leading to the increase of the oscillation amplitude of the second term of Eq. (1) and, thus, AL. Therefore, the contribution of t_{so} can be represented by L_φ/L'_φ. We selected this L_φ/L'_φ as the fitting parameter.

As shown by the dashed line in Fig. 2, the measurement and calculation results are in good agreement in all the samples. This is interpreted as strong evidence for AAS oscillations. The best fittings to Figs. 2(a) and 2(b) give $L_\varphi/L'_\varphi = 1$, assuming $L_\varphi = 10^{-5}$ m and $\beta = 2$. This strongly supports the absence of the SOI and the presence of WL for the reason mentioned above. In particular, the measurement and calculation results are in excellent agreement in Fig. 2(a). On the other hand, both Figs. 2(c) and 2(d) are fitted by two independent oscillation modes depending on the magnetic field (i.e., bimodal behavior) as shown by lines *A* and *B*, assuming finite values for t_{so}. Compared with the value of L_φ/L'_φ of the carbon electrode sample, the best fittings give $L_\varphi/L'_\varphi = 9.18$ and $L_\varphi/L'_\varphi = 9.3$ for lines *A* and *B* in Fig. 2(c) and $L_\varphi/L'_\varphi = 9.28$ and $L_\varphi/L'_\varphi = 9.4$ for lines *A* and *B* in Fig. 2(d), respectively. These values of $L_\varphi/L'_\varphi \sim 9 (>1)$ are strong evidence for the contribution of the SOI and, hence, the emergence of AL, also for the reason explained above. The comment for the bimodal behavior is mentioned in the later part of this paper.

The central issue of this report is the physical relevance of L_φ/L'_φ, as obtained from the best fit shown in Fig. 2, because Eqs. (1)–(4) do not relate to actual material parameters. Two facts make it possible to physically identify this L_φ/L'_φ: (1) there is a correlation with the atomic numbers of the electrode materials (i.e., mass of the atoms) (2) also with the volume ratio of the diffusion region to the MWNT.

From the view point of correlation (1), the atomic numbers (Z's) of C and Pt are 6 and 78. Reference 15 indicates that t_φ/t_{so} is given by $(3L_\varphi^2/al)(aZ)^4$, where a is the fine structure constant ($\approx 1/137$). In the case of carbon, t_φ/t_{so} can be estimated to be on the order of 10^{-6} in our system from this equation. This is nearly consistent with $t_{so} = \infty$ (i.e., $L_\varphi/L'_\varphi = 1$) obtained from the best fits in Figs. 2(a) and 2(b). In contrast, in the case of Pt, t_φ/t_{so} can be estimated to be on the order of 10^{-2}. This does not quantitatively agree with $t_\varphi/t_{so} \approx 5$ estimated from $L_\varphi/L'_\varphi \approx 10$ obtained from the data fitting. In this case, only the increase of t_φ/t_{so} with the atomic number is in qualitative agreement. Hence, based only on Ref. 15, the physical meanings of L_φ/L'_φ cannot be quantitatively identified from the atomic numbers.

In order to clarify correlation (2), we varied the diffusion volume ratio by changing the MWNT length with a constant diffusion length in the same electrode-material samples. L_φ/L'_φ was obtained from the best fit of the experimental data in Figs. 3(c) and 3(d) by Eqs. (1)–(4), by identifying each MWNT length with L_S in Eq. (1). As shown in Fig. 3(b), the relation between the L_φ/L'_φ values and the diffusion volume ratio is mostly linear. This is the strong evidence that the factor of two is the key to determine L_φ/L'_φ (i.e., the contribution of the SOI) and L_φ/L'_φ has a correlation with actual systems. It implies that the contribution of the SOI to AL is linearly proportional to the volume ratio of the diffused Au atom.

Consequently, the diffusion of heavy-mass atoms, deposited as the electrode materials on MWNT's, at only about 5% in volume ratio can drastically change WL to AL in the bulk of NT's. This can be shown by a phase shift of the electron waves by π, caused by spin flipping due to the SOI in the diffusion region of MWNT bulk. However, which conjugated conditions are formed between the atom of Au or Pt and the carbon nanotube by annealing and how it leads to the SOI is still an open question. Further investigation is indispensable to clarify this issue.

Based on the linear relation mentioned above, the bimodal behaviors and the two different L_φ/L'_φ values obtained in Figs. 2(c) and 2(d) suggest the presence of two different distribution peaks in the diffusion volume of Au and Pt atoms in one array sample. The equal ratio of L_φ/L'_φ from line *B* to line *A* (~ 1.013) in both (c) and (d) also supports this conclusion. As a confirmation, we exactly investigated the distribution of diffusion volume ratio in an array. As shown in Fig. 1(d), we could actually find two peaks at 4.9% and 5.1% of the volume ratio. Since the ratio of 5.1%/4.9% is 1.041, this is nearly consistent with the L_φ/L'_φ ratio between

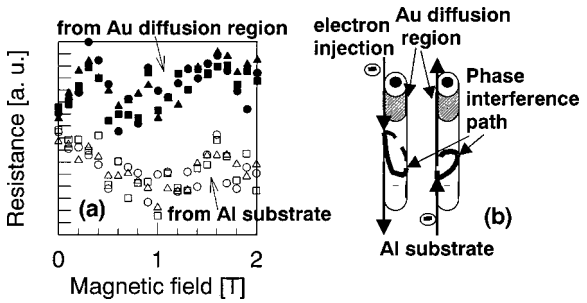

FIG. 4. (a) MR features when electrons are injected from different electrode sides. Open and solid symbols are the MR's for the electron injection from the Al substrate and the Au electrode, respectively. (b) Schematic figures of MWNT's with the phase interference path, encircling the MWNT, for AAS oscillations and the direction of electron injection. Left and right figures mean the electron injections from the Au-diffusion region and Al-substrate sides, respectively.

lines A and B (~ 1.013). However, the reason why they independently emerge in the different magnetic-field regions is still unclear.

Finally, we show why such a small diffusion region only at the one end of the MWNT drastically changes the phase interference in the bulk of the MWNT. Figure 4(a) shows MR oscillations when electrons are injected into the MWNT's from either the Au electrode or Al substrate. It reveals a polarity of AL and WL; i.e., only when electrons are injected through the Au diffusion region does a positive MR (i.e., AL) emerge. This strongly supports the contribution of the SOI caused in the diffusion region. As shown in Fig. 4(b), when the electrons are injected through the Au diffusion region, the electron phases are spin flipped by the strong SOI right after the injection, and then they cause phase interference. Since the spin coherence is strongly conserved in all the phase interference paths of electron waves encircling the MWNT,[11] it leads to the AL in the bulk of the MWNT's. In contrast, when the electrons are injected from the Al substrate, they are spin flipped in the diffusion region, after most of the interference procedure is completed (i.e., after the interference paths were already closed) as shown in (b). Such electrons no longer contribute to the phase interference. These phenomena are the direct evidence of an important role played by the small diffusion region in the phase interference in the bulk of the MWNT's.

We thank C.M. Marcus, L.P. Kouwenhoven, J.P. Leburton, and W. Oliver for useful discussions and suggestions, the MST for the clear TEM image, and J.M. Xu group for the SEM image preparation. This work was financially supported by the MST foundation and the research project grant-in-aid for scientific research of the Japanese Ministry of Education, Science, Sports, and Culture.

[1] S. Kazaoui *et al.*, Phys. Rev. B **60**, 13 339 (1999); R.S. Lee *et al.*, Nature (London) **388**, 255 (1997).
[2] L. Langer *et al.*, Phys. Rev. Lett. **76**, 479 (1996).
[3] S.N. Song *et al.*, Phys. Rev. Lett. **72**, 697 (1994).
[4] V. Bayot *et al.*, Phys. Rev. B **40**, 3514 (1989).
[5] A. Bachtold *et al.*, Nature (London) **397**, 673 (1999).
[6] A. Fujiwara *et al.*, Phys. Rev. B **60**, 13 492 (1999).
[7] J. Haruyama, I. Takesue, T. Hasegawa, and Y. Sato, Phys. Rev. B **63**, 073406 (2001)
[8] J. Haruyama, I. Takesue, and Y. Sato, Appl. Phys. Lett. **77**, 2891 (2000).
[9] J. Haruyama, I. Takesue, and Y. Sato, in *Quantum Mesoscopic Phenomena and Mesoscopic Devices in Microelectronics*, edited by I. Kulik and R. Ellialtiogluet, Vol. 559 of *NATO Advanced Study Institute, Series C* (Plenum, New York, 2000), p. 145.
[10] T.W. Ebbesen *et al.*, Nature (London) **382**, 54 (1996).
[11] K. Tsukagoshi *et al.*, Nature (London) **401**, 572 (1999).
[12] P.W. Anderson, Phys. Rev. **109**, 1492 (1958).
[13] E. Abrahams *et al.*, Phys. Rev. Lett. **42**, 673 (1979).
[14] C. van Haesendonck *et al.*, Phys. Rev. B **25**, 5090 (1982).
[15] B.L. Altshuler *et al.*, JETP Lett. **35**, 588 (1982).
[16] D.Y. Sharvin and Y.V. Sharvin, JETP Lett. **34**, 272 (1981).
[17] S. Hikami, A.I. Larkin, and Y. Nagaoka, Prog. Theor. Phys. **63**, 707 (1980).
[18] F. Komori, S. Kobayashi, and W. Sasaki, J. Phys. Soc. Jpn. **51**, 3136 (1982).
[19] G. Bergman, Phys. Rev. Lett. **48**, 1046 (1982).
[20] C. Papadopoulos *et al.*, Phys. Rev. Lett. **85**, 3476 (2000).